PHYSICAL REVIEW A **77**, 061801(R) (2008)

Efficient energy transfer between four-wave-mixing and six-wave-mixing processes via atomic coherence

Yanpeng Zhang,[1,2,*] Blake Anderson,[1] and Min Xiao[1,†]
[1]*Department of Physics, University of Arkansas, Fayetteville, Arkansas 72701, USA*
[2]*Key Laboratory for Physical Electronics and Devices of the Ministry of Education, Xi'an Jiaotong University, Xi'an 710049, China*
(Received 5 January 2008; published 2 June 2008)

We demonstrate efficient energy exchange during propagation between four-wave-mixing (FWM) and six-wave-mixing (SWM) signals generated in a four-level inverted-Y atomic system, which fall in the electromagnetically induced transparency window. After an initial growth distance for both FWM and SWM fields in the atomic medium, these two nonlinear optical processes compete and exchange energy between them, and eventually reach their respective steady-state values at long interaction distance. This energy exchange phenomenon can be explained by considering established atomic coherences among various atomic states and quantum interferences between three-photon and five-photon excitation pathways. Understanding these high-order nonlinear optical processes and interplays between them can be very important for correlated FWM (or SWM) photon-pair generations and quantum information processing.

DOI: 10.1103/PhysRevA.77.061801 PACS number(s): 42.50.Gy, 42.25.Hz, 42.65.−k

Enhanced four-wave-mixing (FWM) processes in three- and four-level atomic systems due to atomic coherence have attracted a lot of attention in recent years [1–11]. Interesting effects such as ultraslow propagation of matched pulses [6], phase-controlled light switching at low light level [7], quantum destructive interference in inelastic two-wave mixing [8], and generation of correlated photon pairs [9–11] have been experimentally demonstrated in various coherently prepared multilevel atomic systems. These effects depend critically on the interactions and effective couplings between the involved laser beams, and, therefore, the interaction length (or propagation distance) can be important for the systems to reach their equilibrium states [6–8] or to optimize the desired effects. For example, the group velocities of the probe and conjugate pulses only become matched after a certain propagation distance [6] and the rate of photon-pair generation gets higher for larger optical density (OD) of the atomic medium [5,10]. The propagating fields reach equilibrium states (no change afterward) as a result of competitions or interferences between different field-generating processes during their propagation through the medium [6–8]. In the case of matched FWM pulses, the balance is reached between the probe field and the generated conjugate field [6]; in the two-wave-mixing experiment, it is the destructive interference between the source field and the internally generated two-wave-mixing field [8]; and in the case of phase-controlled switching, the constructive and destructive interferences are achieved between the one-photon and three-photon excitation pathways, respectively [7].

On the other hand, earlier experiments have shown that higher-order nonlinear wave-mixing processes, such as six-wave mixing (SWM), can coexist with FWM processes in appropriately selected four-level atomic systems [12–14]. By arranging laser beams in a spatially designed square-box pattern and with certain intensities, the generated SWM signal intensity can be made to be comparable with the FWM signal intensity, which can be made to interfere with each other in frequency [12–14]. In those earlier experiments, no propagation effects were considered since the atomic medium was always kept at high temperature, which causes it to be in the large OD limit for the atomic medium, and the system has already reached equilibrium under such a condition.

In this Rapid Communication, we report our experimental and theoretical studies of how the FWM and SWM signal fields reach their steady-state values during propagation. By manipulating the atomic coherence and quantum interference between different energy levels in the multilevel atomic system with carefully designed phase-matching conditions and intensities, as well as setting the optical depth of the atomic medium at a certain value, we can generate and control coexisting FWM and SWM processes, and their relative strengths. Clear energy transfer between the FWM and SWM signals during their propagation has been observed, and the coupled equations for the probe, FWM, and SWM fields are used to explain the measured results. Studying such energy exchange during propagation between high-order nonlinear wave-mixing processes (which has not been done before) can help us to understand and control these higher-order nonlinear optical processes, and hopefully lead to interesting applications in optoelectronic devices, two-dimensional soliton formation, generations of entangled photons, and quantum information processing [15].

Let us consider a four-level inverted-Y-type atomic system [13,16] with five laser beams, as shown in Fig. 1(a). The probe beam E_p (ω_1, $\mathbf{k}_p$, and Rabi frequency G_p) connects the transition $|0\rangle$ to $|1\rangle$. Two coupling beams, E_2 (ω_2, $\mathbf{k}_2$, and Rabi frequency G_2) and E_2' ($\omega_2, \mathbf{k}_2', G_2'$), interact with the upper transition $|1\rangle$ to $|2\rangle$. Another two pumping beams, E_3 ($\omega_3, \mathbf{k}_3, G_3$) and E_3' ($\omega_3, \mathbf{k}_3', G_3'$), link the transition $|3\rangle$ to $|1\rangle$. When these five laser beams propagate in a spatially designed configuration, as shown in Fig. 1(b), (with $\mathbf{k}_2$ and $\mathbf{k}_3$ traveling in opposite direction of $\mathbf{k}_p$, and $\mathbf{k}_2'$ and $\mathbf{k}_3'$ in the direction having a small angle θ from $\mathbf{k}_2$ and $\mathbf{k}_3$), several FWM and SWM signals are generated in the directions either backward from $\mathbf{k}_2'$ (denoted as $\mathbf{k}_m$ with an angle θ) or with an angle 2θ from $\mathbf{k}_p$ (shown as $\mathbf{k}_s$) according to the phase-

*ypzhang@mail.xjtu.edu.cn
†mxiao@uark.edu

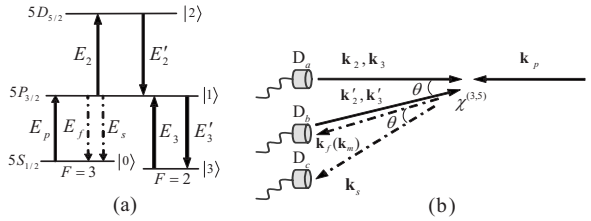

FIG. 1. (a) Four-level atomic system for generating coexisting FWM and SWM processes. The dash-dotted lines are the generated FWM (E_f) and SWM (E_s) signals. (b) Projection of the spatial square-box pattern on a plane for the laser beams used in the experiment [13].

matching conditions [12–14]. Actually, the laser beams are arranged in a square-box pattern as used in Ref. [13], but to simplify the discussion here, we will only be concerned with the different angles on the projected plane as shown in Fig. 1(b). When E_3 and E_3' are blocked, the ladder-type system ($|0\rangle$-$|1\rangle$-$|2\rangle$) generates a FWM signal in the direction with angle θ from $\mathbf{k}_p$ ($\mathbf{k}_f=\mathbf{k}_p+\mathbf{k}_2-\mathbf{k}_2'$, $\rho_{00}^{(0)}\xrightarrow{\omega_1}\rho_{10}^{(1)}\xrightarrow{\omega_2}\rho_{20}^{(2)}\xrightarrow{-\omega_2}\rho_{10}^{(3)}$). When all five beams are on, SWM signals are generated from different interaction processes. Here, we will only be concerned with the dominant high-order nonlinear processes. From the phase-matching condition $\mathbf{k}_s=\mathbf{k}_p+\mathbf{k}_2-\mathbf{k}_2'+\mathbf{k}_3-\mathbf{k}_3'$, efficient SWM signals can be generated via either $\rho_{00}^{(0)}\xrightarrow{\omega_1}\rho_{10}^{(1)}\xrightarrow{\omega_2}\rho_{20}^{(2)}\xrightarrow{-\omega_2}\rho_{10}^{(3)}\xrightarrow{-\omega_3}\rho_{30}^{(4)}\xrightarrow{\omega_3}\rho_{10}^{(5)}$ or $\rho_{00}^{(0)}\xrightarrow{\omega_1}\rho_{10}^{(1)}\xrightarrow{-\omega_3}\rho_{30}^{(2)}\xrightarrow{\omega_3}\rho_{30}^{(3)}\xrightarrow{\omega_2}\rho_{20}^{(4)}\xrightarrow{-\omega_2}\rho_{10}^{(5)}$, which are both in the direction of the 2θ angle from $\mathbf{k}_p$ (denoted as $\mathbf{k}_s$ and E_s with frequency ω_1 in Fig. 1). At the same time, other SWM processes (using one photon each from E_p, E_3, E_3', but two photons either from E_2 or E_2') can exist and propagate in the direction of $\mathbf{k}_m$, which can produce interference between colinear FWM and SWM processes [13].

However, in the current experiment we try to separate the FWM and SWM signals, so the SWM signals propagating collinearly with FWM (in the $\mathbf{k}_m$ direction) have been intentionally suppressed by using lower E_2 and E_2' in comparison with E_3 and E_3', and by carefully misaligning the E_3 and E_3' beams slightly, so in the $\mathbf{k}_m$ direction the FWM signal dominates, and we can denote $\mathbf{k}_m\approx\mathbf{k}_f$. Although FWM ($\mathbf{k}_f$) and SWM ($\mathbf{k}_s$) signals travel in different directions (with a small angle θ between them), they share the same fields E_p, E_2, and E_2'. Both the generated FWM and SWM signals are in the same electromagnetically induced transparency (EIT) window formed by the ladder system ($|0\rangle\rightarrow|1\rangle\rightarrow|2\rangle$) in two-photon Doppler-free configuration [17] and have the same frequency (ω_1) as the probe beam. In the generated FWM and SWM signal beams, the coherence lengths are given by $l_c^f=2c/[n(\omega_2/\omega_1)|\omega_2-\omega_1|\theta^2]$ and $l_c^s=2c/\{n[(\omega_2+\omega_3)/\omega_1]|\omega_2+\omega_3-\omega_1|\theta^2\}$, respectively, with n being the refractive index at the frequency ω_1. In our experiment, θ is very small (about 0.3°) so that l_c^f and l_c^s are much larger than the interaction length L, so the phase mismatch can be neglected.

Under the conditions $G_3, G_3' > G_2, G_2' \gg G_p$, a set of coupled equations for the probe field and the generated dominant FWM and SWM fields can be used to describe the dynamics of the system as

$$\partial G_p/\partial z = i\xi_p\rho_{10}^p = -\frac{D_1}{D_l}G_p + \frac{D_2}{D_f}G_f\exp(-i\Delta\mathbf{k}_f\cdot\mathbf{r}) - \frac{D_3}{D_s}G_s\exp(-i\Delta\mathbf{k}_s\cdot\mathbf{r}), \tag{1a}$$

$$\partial G_f/\partial z = i\xi_f\rho_{10}^f = -\frac{D_4}{D_l}G_f + \frac{D_5}{D_f}G_p\exp(i\Delta\mathbf{k}_f\cdot\mathbf{r}) + \frac{D_6}{D_f}G_s\exp(i\Delta\mathbf{k}_s\cdot\mathbf{r}), \tag{1b}$$

$$\partial G_s/\partial z = i\xi_s\rho_{10}^s = -\frac{D_7}{D_l}G_s - \frac{D_8}{D_s}G_p\exp(i\Delta\mathbf{k}_f\cdot\mathbf{r}) - \frac{D_8}{D_s}G_f\exp(i\Delta\mathbf{k}_s\cdot\mathbf{r}), \tag{1c}$$

where $\xi_{p(f,s)}\equiv 2\mathbf{k}_{p(f,s)}\mu^2N/\hbar$, $\Delta\mathbf{k}_f=\mathbf{k}_1-\mathbf{k}_f$, $\Delta\mathbf{k}_s=\mathbf{k}_1-\mathbf{k}_s$. When the laser beams are on resonances, $D_1=\xi_p\Gamma_{20}\Gamma_{30}$, $D_2=\xi_p\Gamma_{30}G_2^2$, $D_3=\xi_pG_2^2G_3^2$, $D_4=k_fD_1/k_p$, $D_5=k_fD_2/k_p$, $D_6=k_fG_3^2D_2/(G_2^2k_p)$, $D_7=k_sD_1/k_p$, $D_8=k_sG_3^2D_2/(\Gamma_{30}k_p)$, $D_l=\Gamma_{10}\Gamma_{20}\Gamma_{30}+\Gamma_{30}G_2^2+\Gamma_{20}G_3^2$, $D_f=\Gamma_{10}\Gamma_{20}(\Gamma_{10}\Gamma_{30}+G_3^2)$, and $D_s=\Gamma_{10}^3\Gamma_{20}\Gamma_{30}$. N, Γ_{mn}, $\Delta_i=\Omega_i-\omega_i$, and μ are the atomic density, decoherence rates, frequency detunings from the atomic resonant frequency Ω_i, and the dipole moment of the relevant transition, respectively.

Equations (1a)–(1c) are derived from the optical responses of the medium to the probe, the generated FWM, and SWM fields, respectively. The first terms in these equations contain the linear susceptibilities with the EIT signature, and the second and third terms in each equation are contributions from the third- and fifth-order nonlinear susceptibilities, respectively, which are the parametric conversion processes More explicitly, the linear susceptibilities control the dispersion profiles and transmission spectra of the probe and the generated FWM and SWM fields, while the third- and fifth-order nonlinearities play essential roles in determining the features of energy transfer between these FWM and SWM processes.

These coupled equations indicate that not only can the probe beam can generate FWM and SWM fields, but these FWM and SWM fields can also affect each other as well as the probe beam via reabsorption and backward nonlinear processes during their propagation [6–8]. Competitions between these fields are the key to establishing the equilibrium among them. The solutions of these coupled equations determine the propagation characteristics of the generated E_f and E_s fields. To see the physical picture more clearly without giving complicated solutions, we rewrite Eqs. (1b) and (1c) as

$$\partial(G_f+G_s)/\partial z = -\frac{D_4}{D_l}(G_f+G_s) + \left(\frac{D_5}{D_f}-\frac{D_8}{D_s}\right)G_p + \left(\frac{D_6}{D_f}G_s - \frac{D_8}{D_s}G_f\right). \tag{2}$$

By examining the solutions at large propagation distance (which give $D_1\approx D_4\approx D_7$ and $D_3\approx D_8$), we notice that some

balance conditions are satisfied, i.e., $D_2G_f/D_f-D_3G_s/D_s=0$ in Eq. (1a) for the probe beam, and $D_6G_s/D_f-D_8G_f/D_s=0$ in Eq. (2) for the FWM+SWM signals. Quantum destructive interferences between three-photon (G_f) and five-photon (G_s) excitation pathways are the underlying mechanisms for the probe and the generated FWM+SWM signals to reach equilibrium.

For given initial conditions of $G_p(z=0)=Q_0$, $G_f(z=0)=G_s(z=0)=0$ at the entrance face of the medium, Eqs. (1a) and (2) can be solved analytically to be

$$G_f+G_s=\frac{Q_0D_l}{D_1-D_4}\left(\frac{D_8}{D_s}-\frac{D_5}{D_f}\right)\left[1-\exp\left(-\frac{D_4z}{D_l}\right)\right], \quad (3)$$

where $D_4z/D_l \propto Nz$. From Eq. (3), it is clear that for sufficiently large Nz with $\exp(-D_4z/D_l) \ll 1$, the solution reaches a constant value independent of z. These balancing conditions indicate that after an initial propagation distance for the FWM and SWM signals to build up (while the probe intensity decreases accordingly), the probe beam and the total generated FWM+SWM beams reach their equilibrium. After that, the FWM and SWM fields will only transfer energies between themselves and, eventually, after a much longer propagation distance, reach their individual steady states, so they will propagate in the medium without further absorption and distortion

The experiment was performed using ^{85}Rb atoms in an atomic vapor cell (length 5 cm). The relevant energy levels are $5S_{1/2}$, $F=3$ ($|0\rangle$), $5S_{1/2}$, $F=2$ ($|3\rangle$), $5P_{3/2}$ ($|1\rangle$), and $5D_{5/2}$ ($|2\rangle$), which form the inverted-Y atomic system, as shown in Fig. 1(a). An extended cavity diode laser (ECDL) provides the radiation for the probe field E_p at 780.24 nm. The radiation of another ECDL at 775.98 nm is split to yield the two coupling beams E_2 and E_2'. The radiation of a cw Ti:sapphire laser at 780.23 nm is split to yield the two pump beams E_3 and E_3'. Since the propagation factor in the solution of Eqs. (1) and (2) is proportional to Nz, an easier way to change the "effective propagation length (Nz)" is to change the atomic density N by changing the temperature of the atomic cell, and keep the atomic cell length (z) fixed as L [6–8]. Three detectors were set at three different directions: D_a in the direction of the probe beam to monitor the probe transmission, D_b at angle θ to detect the dominant FWM signal, and D_c at angle 2θ to detect the SWM signal, respectively. The detected probe transmission, FWM, and SWM signals are depicted in Fig. 2. At low temperature, there is a ladder-type EIT window [Fig. 2, (a3)] due to the two-photon Doppler-free configuration in this setup [17]. However, at high temperature, the EIT window becomes an absorption peak [Fig. 2, (b3)]. By carefully aligning all the laser beams in the square-box pattern [Fig. 1(b) and Ref. [13]] and selectively blocking different laser beams, the generated FWM [curves (a2) and (b1)] and SWM [curves (a1) and (b2)] signals are identified. There is a small SWM component in curves (a2) and (b1) of Fig. 2 [13], which is more than ten times smaller than the FWM signal of interest and, therefore, can be neglected in our current discussion. The powers of the coupling and pumping beams E_2 (E_2') and E_3 (E_3') are 15 and 65 mW, respectively. The corresponding frequency detunings of the beams E_2 (E_2') and E_3 (E_3') are 312 and 0 MHz. The probe beam is set at 0.7 mW to optimize the generated FWM and SWM signals.

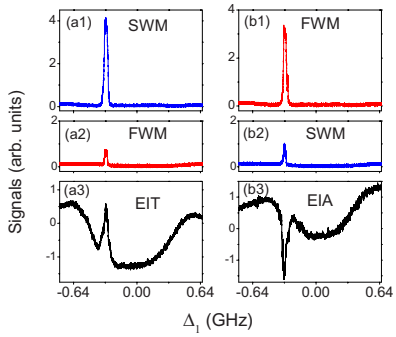

FIG. 2. (Color online) Measured coherently enhanced FWM and SWM signal intensities, and the corresponding probe beam transmission for selected atomic densities ($0.2\times10^{12}/\mathrm{cm}^3$ [curves (a1)–(a3)] and $1.1\times10^{12}/\mathrm{cm}^3$ [curves (b1)–(b3)]) versus probe detuning Δ_1. The experimental parameters are $G_1=2\pi\times5$ MHz, $G_2=G_2'=2\pi\times35$ MHz, $G_3=G_3'=2\pi\times80$ MHz, $\Delta_3=0$, and $\Delta_2=312$ MHz.

Figure 3 (square points) shows the intensities of the probe, FWM, and SWM signals as a function of atomic density, respectively. The FWM and SWM signals increase initially at low atomic density (or equivalently short propagation distance) as the probe beam intensity decreases. At certain optical density (about $N=0.3\times10^{12}/\mathrm{cm}^3$), the probe and the FWM+SWM intensities reach their equilibrium, after which energy exchange occurs only between the FWM and SWM signals as they propagate through the medium. Eventually, at a higher atomic density (about $N=1.2\times10^{12}/\mathrm{cm}^3$), the FWM and SWM signals reach their respective steady-state values individually. This is the first such observation of energy exchange between the generated FWM and SWM signals in propagation and the process of reaching their steady-state values. The theoretically simulated results from Eq. (1) are plotted in Fig. 3 (solid lines), and match quite well with the measured data.

Such energy exchange during propagation can be influenced by many parameters. For example, the intensities of E_3 and E_3' can greatly modify the balance between the FWM

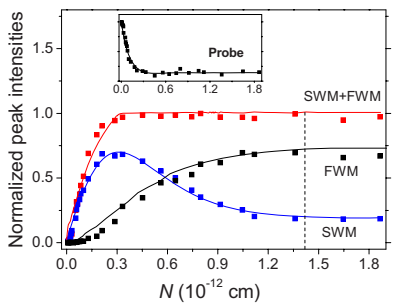

FIG. 3. (Color online) Square points: Measured FWM and SWM peak intensities versus atom number density (FWM curve, SWM curve, and FWM+SWM curve). Inset: The measured probe intensity at the EIT window. Solid lines: Theoretically calculated curves corresponding to the measured results (square points). The parameters are $G_1=2\pi\times5$ MHz, $G_2=G_2'=2\pi\times35$ MHz, $G_3=G_3'=2\pi\times80$ MHz, $\Delta_3=0$, $-\Delta_1=\Delta_2=312$ MHz, $\Gamma_{10}/2\pi=3$ MHz, $\Gamma_{20}/2\pi=0.4$ MHz, and $\Gamma_{30}/2\pi=2$ MHz.

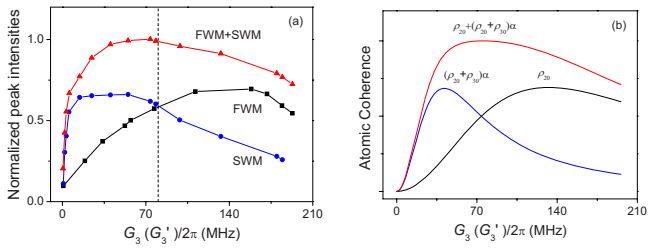

FIG. 4. (Color online) (a) Measured FWM and SWM peak intensities, as well as the total FWM+SWM intensity, versus the pump field G_3 (G_3'). (b) Theoretically calculated atomic coherences [ρ_{20} curve, $(\rho_{20}+\rho_{30})\alpha$ curve, and $\rho_{20}+(\rho_{20}+\rho_{30})\alpha$ curve] versus pump field G_3 (G_3'). The parameters are $G_1=2\pi\times 5$ MHz, $G_2=G_2'=2\pi\times 35$ MHz, $N=1.4\times 10^{12}/\mathrm{cm}^3$, $\Delta_3=0$, $-\Delta_1=\Delta_2=312$ MHz, $\Gamma_{10}/2\pi=3$ MHz, $\Gamma_{20}/2\pi=0.4$ MHz, and $\Gamma_{30}/2\pi=2$ MHz.

and SWM generating processes. By fixing the atomic cell temperature to have $N=1.4\times 10^{12}/\mathrm{cm}^3$ (dashed line in Fig. 3), the relative FWM and SWM intensities can be tuned by varying the power of E_3 (E_3'). Figure 4 shows the generated FWM and SWM signal intensities as a function of G_3 (G_3'). The behaviors shown here are not governed by Eq. (1), where large G_3 and G_3' are assumed. It is interesting to notice that as E_3 (and E_3') is turned on from zero, SWM intensity increases very rapidly to a maximal value, and then decreases steadily as the pump beam power increases further. At the same time, FWM signal power increases slowly up to a quite large value before decreasing. The FWM process in the ladder system is modified due to the dressing by the E_3 and E_3' fields. The top curve in Fig. 4(a) is the sum intensity of the FWM and SWM signals, which has the same behavior as the calculated total atomic coherence of $\rho_{20}+(\rho_{20}+\rho_{30})\alpha$ [Fig. 4(b)] (α is the ratio between the fifth-order and third-order susceptibilities) by using the full density-matrix equations, thereinto, FWM and SWM correspond to the atomic coherence ρ_{20} [8] and $(\rho_{20}+\rho_{30})\alpha$, respectively. Figure 3 takes the value of $G_3=2\pi\times 80$ MHz (at which the FWM and SWM signals have the same value) [dashed line in Fig. 4(a)]. Such comparisons indicate that the atomic coherences play significant roles in the enhancements of high-order multi-wave mixing processes and in the process of establishing equilibrium for the generated FWM and SWM signals during propagation.

There are a few important issues that are worth raising here. First, if a pulsed laser is used for the probe beam, the generated FWM and SWM signals will be slowed down due to sharp dispersion, and eventually become pulse-matched with the probe pulses, as in the case of FWM [6]. Such a system could possibly be used to generate entangled FWM (or SWM) photon pairs and even triplet photons for quantum information processing [15]. Second, both FWM and SWM processes described here share the same E_p, E_2, and E_2' beams, so strong competitions between these wave-mixing processes, as well as the three-photon and five-photon interferences, exist in this system. The energy exchange and interactions between the generated FWM and SWM during propagation are the manifestation of strong coupling and competitions between these high-order nonlinear optical processes. Third, in order to investigate the FWM and SWM energy exchange, we selectively suppressed the typically efficient SWM channels in the k_m direction [13] (by using lower E_2 and E_2' powers and slightly misaligning the E_3 and E_3' beams), so only the dominant FWM process needs to be considered in this direction.

In summary, FWM and SWM processes were shown to coexist in the inverted-Y atomic system. The efficient coupling between these high-order nonlinear wave-mixing processes makes them exchange energy in propagation before reaching their respective equilibrium values at long propagation distance (or high optical density) through the medium. Quantum destructive interferences between three-photon and five–photon excitation pathways for FWM and SWM, respectively, as well as reabsorption via nonlinear processes, are the underlying mechanism for the generated FWM and SWM fields to reach equilibrium. By choosing appropriate propagation length (or atomic cell temperature) or pump power E_3 and E_3', one can get desired relative strengths between the FWM and SWM signals from $I_{\mathrm{FWM}}<I_{\mathrm{SWM}}$ to $I_{\mathrm{FWM}}>I_{\mathrm{SWM}}$. A theoretical model has been developed to compare with the experimentally measured FWM and SWM generation processes during propagation with excellent agreements. Understanding and controlling the high-order nonlinear optical processes, such as $\chi^{(3)}$ and $\chi^{(5)}$, can be very important in studying new physical phenomena (such as two-dimensional soliton formation and liquid light condensate) and in designing new applications for quantum information processing (such as entangled photon generations and three-qubit quantum computation) [9–11,15,18].

We acknowledge funding support from the National Science Foundation.

[1] P. R. Hemmer *et al.*, Opt. Lett. **20**, 982 (1995).
[2] Y. Li and M. Xiao, Opt. Lett. **21**, 1064 (1996).
[3] B. Lu *et al.*, Opt. Lett. **23**, 804 (1998).
[4] M. M. Kash *et al.*, Phys. Rev. Lett. **82**, 5229 (1999).
[5] D. A. Braje *et al.*, Phys. Rev. Lett. **93**, 183601 (2004).
[6] V. Boyer *et al.*, Phys. Rev. Lett. **99**, 143601 (2007).
[7] H. Kang *et al.*, Phys. Rev. A **73**, 011802(R) (2006).
[8] K. J. Jiang *et al.*, Phys. Rev. Lett. **98**, 083604 (2007).
[9] V. Balic *et al.*, Phys. Rev. Lett. **94**, 183601 (2005).
[10] S. W. Du *et al.*, Phys. Rev. Lett. **98**, 053601 (2007).
[11] C. F. McCormick *et al.*, Opt. Lett. **32**, 178 (2007).
[12] Y. P. Zhang *et al.*, Phys. Rev. Lett. **99**, 123603 (2007).
[13] Y. P. Zhang and M. Xiao, Appl. Phys. Lett. **90**, 111104 (2007).
[14] Y. P. Zhang *et al.*, Opt. Lett. **32**, 1120 (2007).
[15] H. Michinel *et al.*, Phys. Rev. Lett. **96**, 023903 (2006); Y. Wu and L. Deng, *ibid.* **93**, 143904 (2004); J. M. Wen *et al.*, Phys. Rev. A **77**, 033816 (2008).
[16] M. Yan *et al.*, Phys. Rev. A **64**, 043807 (2001); A. Joshi and M. Xiao, Phys. Lett. A **317**, 370 (2003).
[17] S. E. Harris, Phys. Today **50** (7), 36 (1997); J. Gea-Banacloche *et al.*, Phys. Rev. A **51**, 576 (1995).
[18] D. J. Ulness *et al.*, J. Chem. Phys. **108**, 3897 (1998); K. D. Moll *et al.*, Phys. Rev. Lett. **88**, 153901 (2002).